NANOPARTICLE-INDUCED CATALYTIC CARBON CAPTURE: A MICROFLUIDICS APPROACH

by

Joshua Donjuan

A Thesis Submitted to the Faculty of

College of Engineering and Computer Science

In Partial Fulfillment of the Requirements for the Degree of

Master of Science

Florida Atlantic University

Boca Raton, FL

August 2024

NANOPARTICLE-INDUCED CATALYTIC CARBON CAPTURE: A

MICROFLUIDICS APPROACH

by

Joshua Donjuan

This thesis was prepared under the direction of the candidate's thesis advisor, Dr. Myeongsub Kim, Department of Mechanical Engineering, and has been approved by all members of the supervisory committee. It was submitted to the faculty of the College of Engineering and Computer Science and was accepted in partial fulfillment of the requirements for the degree of Master of Science

SUPERVISORY COMMITTEE:

Myeongsub Kim
Myeongsub Kim (Jul 17, 2024 14:45 EDT)

Myeongsub Kim, Ph.D.
Thesis Advisor

tsung-chow Su
tsung-chow Su (Jul 18, 2024 06:31 GMT+8)

Tsung-Chow Su, Eng. Sc. D.

J W Louda (Jul 17, 2024 18:35 EDT)

J. William Louda, Ph.D.

Pierre Philippe Beaujean

Pierre-Philippe Beaujean, Ph.D.
Chair, Department of Mechanical and Ocean Engineering

Stella Batalama

Stella Batalama, Ph.D.
Dean, College of Engineering and Computer Science

Robert W Stackman

Robert W. Stackman Jr., Ph.D.
Dean, Graduate College

July 19, 2024

Date

ACKNOWLEDGEMENTS

I would like to express my gratitude to my research advisor, Dr. Myeongsub Kim, for giving me the opportunity to work in his lab with continuous support. He has taught me the methodology to carry out the research. It was a great privilege and honor to work under his guidance.

I would like to thank Abishek Pravinbhai Ratanpara for being a supportive research colleague.

Lastly, I want to give thanks to my family for supporting me throughout my time during this degree.

ABSTRACT

Author: Joshua Donjuan

Title: NANOPARTICLE-INDUCED CATALYTIC CARBON CAPTURE: A MICROFLUIDICS APPROACH

Institution: Florida Atlantic University

Thesis Advisor: Dr. Myeongsub Kim

Degree: Master of Science

Year: 2024

Due to technological advancement, energy consumption and demand have been increasing significantly, primarily satisfied by fossil fuel consumption. This reliance on fossil fuels results in substantial greenhouse gas emissions, with CO_2 being the most prominent contributor to global warming. To mitigate this issue and prevent CO_2 emissions, Carbon Capture, Utilization, and Storage (CCUS) technologies are employed. Among these, the amine scrubbing method is widely used due to its high CO_2 capture efficiency and regenerative ability. However, this method has drawbacks, including high toxicity, corrosion, and substantial freshwater consumption.

To develop an environmentally sustainable carbon capture solution, researchers are exploring alternatives such as the use of seawater and enhanced CO_2 capture with catalysts. In this study, we analyze the catalytic performance of nickel nanoparticles (NiNPs) in seawater with carboxymethyl cellulose (CMC) polymers. Using flow-focusing geometry-based microfluidic channels, we investigated CO_2 dissolution at various concentrations of

nanoparticles and CMC polymers. The objective is to optimize the concentration of nanoparticles and CMC polymers for effective CO_2 dissolution. We utilized NiNPs with diameters of 100 nm and 300 nm in CMC concentrations of 100 ml/L, 200 ml/L, and 300 ml/L. Additionally, NiNP concentrations ranging from 6 mg/L to 150 mg/L were tested for CO_2 dissolution in seawater. The results indicated that a concentration of 10 mg/L NiNPs in 100 mg/L CMC provided a CO_2 dissolution of 57%, the highest for this specific CMC concentration. At CMC concentrations of 200 ml/L and 300 ml/L, NiNP concentrations of 70 mg/L and 90 mg/L achieved CO_2 dissolution rates of 58.8% and 67.2%, respectively.

We conclude that at specific CMC concentrations, the NiNP concentration exhibits a bell-shaped curve with optimized values. This unique behavior can potentially aid in the future optimization of NiNPs as catalysts for seawater-based CO_2 capture.

Nanoparticle-Induced Catalytic Carbon Capture: A Microfluidics Approach

LIST OF FIGURES

1. INTRODUCTION

Accompanying technological advancements, global energy demands have been increasing at an unprecedented rate. Currently, most of these energy demands are satisfied by fossil fuels, such as coal, oil, and natural gas. Despite efforts to boost renewable energy production, the reliance on fossil fuels remains significantly high. For instance, in 2019, fossil fuels accounted for approximately 80.9% of global energy consumption [1]. This heavy dependence on fossil fuels poses a serious environmental concern due to the emission of greenhouse gases (GHGs), particularly carbon dioxide (CO_2), which is a major contributor to global warming. CO_2 is responsible for about 76% of total GHG emissions in 2010, making it the primary driver of climate change [5]. To mitigate the adverse effects of CO_2 emissions, various CO_2 capture methods have been developed. The technology of capturing and safely storing CO_2 gas is known as Carbon Capture, Utilization, and Storage (CCUS). CCUS involves a series of processes that capture CO_2 from point sources, such as power plants and industrial facilities, and subsequently store it underground or utilize it in various applications to prevent its release into the atmosphere.

The CO_2 capture process can be mainly divided into three types: pre-combustion capture, post-combustion capture (PCC), and oxy-fuel combustion. Each of these methods has its unique mechanisms and applications. In pre-combustion capture, fuel is gasified to produce a mixture of hydrogen and CO_2, with the CO_2 being separated before the combustion process [4]. Post-combustion capture involves capturing CO_2 from flue gases produced after combustion, making it widely used in major CO_2 emitting plants like coal-based thermal power plants, steel, and concrete manufacturing plants [9]. Oxy-fuel combustion, on the other hand, burns fuel in pure oxygen instead of air, resulting in a flue gas that is mainly CO_2 and water vapor, which can be easily separated [2]. Among these technologies, post-combustion capture is the most practical and widely used method for CO_2 removal in existing fossil fuel power plants. One of the successfully implemented methods in post-combustion capture is called amine scrubbing. In this method, monoethanolamine (MEA) is used for capturing CO_2 due to its high reactivity and selectivity towards CO_2 [8]. However, despite its effectiveness, there are some drawbacks associated with MEA scrubbing, including high energy consumption for the regeneration of MEA, which can reduce the overall efficiency of the power plant [7]. Additionally, MEA is corrosive, necessitating the use of corrosion-resistant materials, which can increase the cost of the capture system [6]. Furthermore, MEA can degrade over time, producing harmful by-products that require additional treatment and disposal [2].

While post-combustion carbon capture remains the most practical and widely used method for CO_2 removal in existing fossil fuel power plants, the environmental and economic challenges associated with MEA scrubbing highlight the need for continued research and development. One promising area of research is the use of nanoparticles as catalysts in the

CO_2 capture process. Nanoparticles have gained a lot of attention due to their large surface area and unique properties that can enhance the efficiency of CO_2 capture [3]. This thesis explores the potential of alternative solvents and advanced materials, including nanoparticles, to offer pathways to more efficient and environmentally benign carbon capture solutions. By leveraging advancements in nanotechnology and materials science, I aim to develop the next-generation CO_2 capture systems that overcome the limitations of current methods and contribute to global efforts in mitigating climate change.

2. LITERATURE REVIEW

2.1 PRE-COMBUSTION CARBON CAPTURE

Pre-combustion carbon capture is a technology aimed at reducing CO_2 emissions from fossil fuel power plants and industrial processes by capturing CO_2 before the fuel is combusted. The process begins with the gasification of fossil fuels, such as coal or natural gas, to produce a synthesis gas (syngas), primarily composed of hydrogen (H_2) and carbon monoxide (CO). This syngas undergoes a water-gas shift reaction, where CO reacts with water vapor to produce additional H_2 and CO_2. The resultant CO_2 is then separated from the hydrogen using physical or chemical absorption methods, such as solvents like amines or pressure swing adsorption. The captured CO_2 can be transported for storage or utilization, while the remaining hydrogen can be used as a clean fuel, producing only water (H_2O) as a byproduct, for power generation or other industrial applications. This process is illustrated in **Figure 1**, which shows a block diagram of the steps involved.

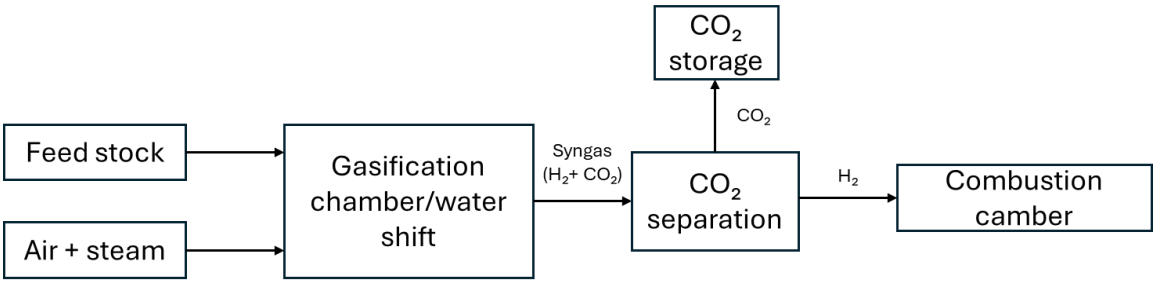

Figure 1: A diagram illustrating Pre-Combustion Carbon Capture.

The primary advantages of pre-combustion carbon capture include higher efficiency in CO_2 removal and reduced energy penalties compared to post-combustion methods. It benefits from the higher concentration and pressure of CO_2 in the syngas, which facilitates easier separation. This method also integrates well with Integrated Gasification Combined Cycle (IGCC) plants, which are known for their high efficiency and low emissions [33,34]. Additionally, pre-combustion capture can significantly reduce the emissions of other pollutants like sulfur oxides and nitrogen oxides due to the inherent gasification process [10,13].

However, there are several drawbacks associated with pre-combustion carbon capture. The complexity and high capital costs of IGCC plants pose significant economic challenges. The need for extensive syngas treatment and the integration of multiple complex processes can lead to higher operational and maintenance costs. Furthermore, while the efficiency of CO_2 capture is high, the overall efficiency of the power plant can be compromised due to the energy required for gasification and CO_2 separation processes [11].

Another disadvantage is the need for large-scale infrastructure to handle and store the captured CO_2. Although promising, the commercial maturity of pre-combustion capture technologies is still limited, with only a few demonstration plants in operation. The development of such plants requires significant investment and time, which can delay the widespread adoption of this technology [12]

2.2 OXYFUEL

Oxyfuel carbon capture is a promising technology designed to reduce CO_2 emissions from power plants by burning fuel with nearly pure oxygen instead of air. This process involves the combustion of fossil fuels in an environment of pure oxygen, producing a flue gas that is primarily composed of CO_2 and water vapor. The water vapor is then condensed out, leaving a stream of almost pure CO_2, which can be compressed and stored or utilized in various industrial processes [14]. The process is illustrated in **Figure 2**, which presents a block diagram of the oxyfuel carbon capture process.

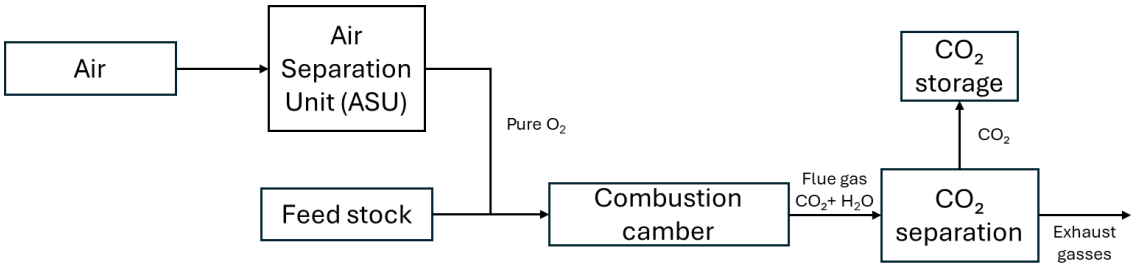

Figure 2: A diagram illustrating Oxyfuel Carbon Capture.

One of the primary advantages of oxyfuel carbon capture is its potential to produce a highly concentrated stream of CO_2, which simplifies the capture process and reduces the costs associated with CO_2 purification and compression. This high concentration of CO_2 in the flue gas can lead to lower costs for CO_2 capture compared to traditional air-fired combustion processes [15].

However, there are also notable disadvantages to oxyfuel carbon capture. One of the major challenges is the energy-intensive nature of the air separation unit (ASU), which is required to produce the pure oxygen needed for combustion. The ASU represents a significant portion of the overall energy penalty associated with oxyfuel combustion, thereby reducing the net efficiency of the power plant [16].

Moreover, the presence of impurities in the CO_2 stream, such as sulfur oxides (SO_x) and nitrogen oxides (NO_x), can pose challenges for CO2 transportation and storage. These impurities may lead to corrosion in pipelines and storage facilities, necessitating additional purification steps and thereby increasing costs [17].

While oxyfuel carbon capture offers significant potential for reducing CO_2 emissions with relatively pure CO2 streams and low NOx emissions, it faces substantial challenges related to energy consumption, system complexity, and impurity management. Continued research and development are essential to overcome these barriers and make oxyfuel carbon capture a viable option for large-scale deployment in power plants [18].

2.3 POST-COMBUSTION CARBON CAPTURE (PCC)

PCC is a crucial technology for reducing CO_2 emissions from industrial and power plant sources because it can be retrofitted to existing plants without major modifications. This flexibility makes PCC an attractive option for immediate and large-scale implementation. Unlike the two options previously proposed, which require significant changes to existing infrastructure.

PCC involves capturing CO_2 from the flue gas produced by the combustion of fossil fuels. The primary methods of post-combustion capture include absorption, adsorption, and

membrane separation. Absorption, the most mature and widely used technique, typically involves chemical solvents such as monoethanolamine (MEA) to capture CO_2 this method is known as amine-scrubbing. The flue gas is passed through a solvent where CO_2 is absorbed, and the solvent is then regenerated to release the captured CO_2 for storage or utilization [19,20]. **Figure 3** illustrates the process of post-combustion carbon capture.

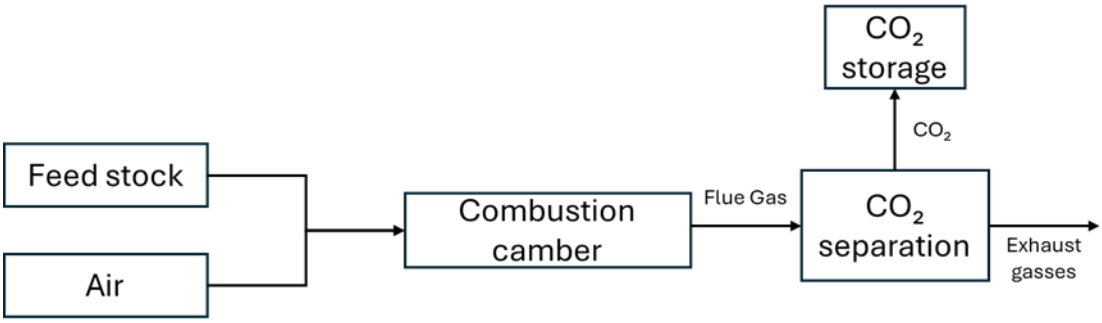

Figure 3: A diagram illustrating Post-Combustion Carbon Capture.

Due to excellent retrofitting ability onto existing plants, amine scrubbing process has been widely accepted method for carbon capture among all options. [21].

This adaptability is crucial for the near-term implementation of CO_2 reduction strategies. Additionally, amine scrubbing can achieve high capture efficiencies, with some systems capable of removing up to 90% of CO_2 from flue gases [22]. Furthermore, the technology is supported by a robust body of research and has seen significant developments over the years, enhancing its feasibility and efficiency [23].

However, amine scrubbing also faces several challenges. One of the primary drawbacks is the high energy requirement for the regeneration of solvents, which can significantly reduce the overall efficiency of power plants [24]. The energy penalty associated with solvent regeneration often translates into increased operational costs and reduced net energy output [25]. Additionally, the implementation of amine scrubbing technologies can

be capital-intensive, posing economic challenges for widespread adoption [21]. Environmental concerns also arise from the potential for solvent degradation and the production of hazardous byproducts, necessitating stringent management and disposal practices [26].

Moreover, different capture methods present specific challenges and advantages. Adsorption processes, for instance, can offer lower energy penalties compared to absorption but often suffer from lower CO_2 capture capacities [27]. Membrane separation technologies are still in the developmental phase and require further advancements to become economically viable at a large scale [19]. Each method requires tailored solutions to address these inherent challenges while improving overall efficiency and reducing costs.

To avoid these drawbacks researchers are seeking more environmentally friendly or environmentally benign solutions. Along the way to achieve the most sustainable solution, implementation of nanoparticles as catalyst has been also investigated such as, use of silica (SiO_2) and aluminum oxide (AL_2O_3) [31]. Moreover, NiNPs are to have shown great potential for their CO_2 capture and regenerative capability [29].

NiNPs have been shown to enhance catalytic performance in CO_2 absorption when used with traditional solvents such as MEA [28,29]. It was found that adding NiNPs to MEA can increase its CO_2 absorption rate by 34% under limited mixing conditions and up to 54% under high mixing conditions **(Figure 4)**. This enhancement is primarily due to the NiNPs, which facilitate faster absorption and can potentially reduce the size of industrial reactors for PCC, leading to lower capital costs [28]. However, in these experiments, DI water was used to suspend the nanoparticles.

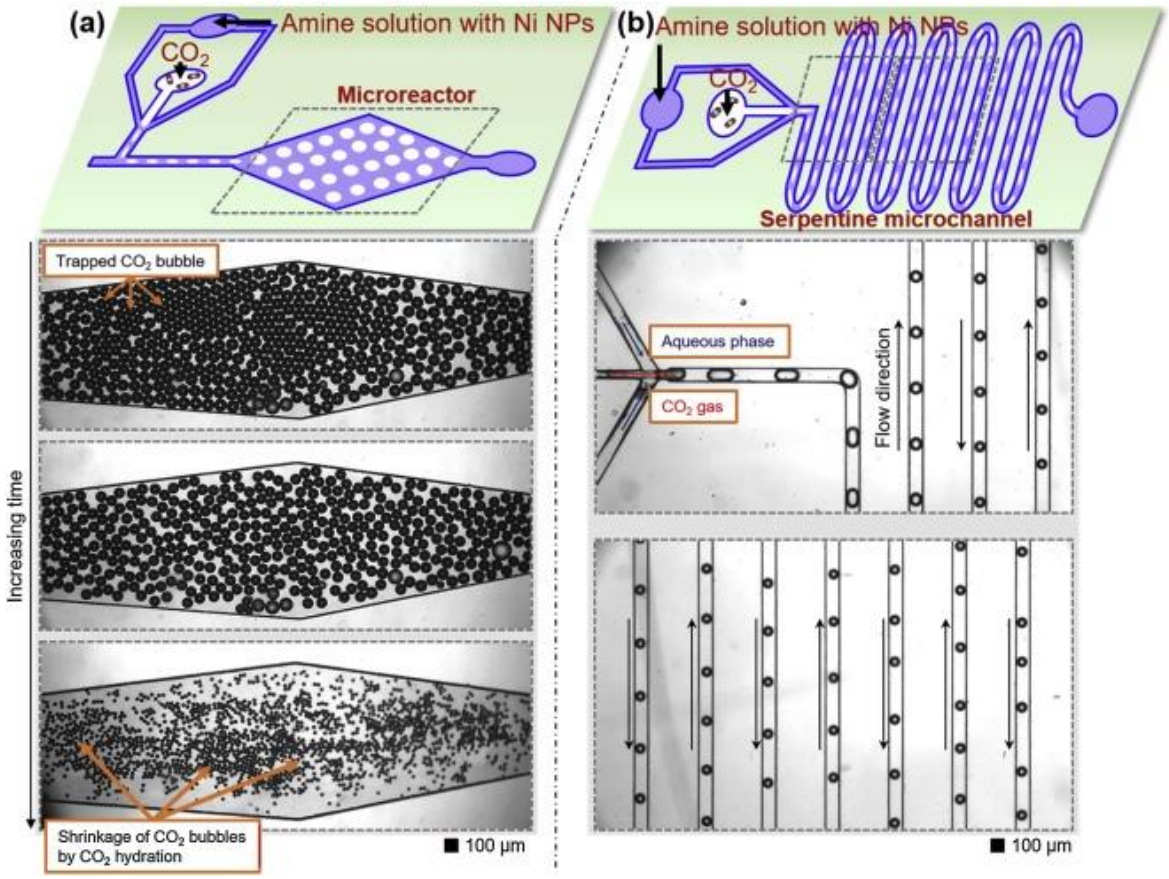

Figure 4: (a) Microfluidic microreactor (low mixing conditions). (b) Design of serpentine microchannel (high mixing condition) [28].

Expanding on the use of NiNPs, a similar experiment was conducted using seawater instead of DI water along with NiNPs and MEA [29]. This study aimed to evaluate the CO_2 capture efficiency using seawater, which contains natural ions such as calcium and magnesium that can react with CO_2 to form carbonate minerals, thereby enhancing the overall absorption process. The experiment found that the combination of NiNPs and 2.5% amine resulted in 97.05% CO_2 absorption in natural seawater. These results suggest that seawater could be a viable alternative to fresh water, reducing the demand for fresh water and potentially lowering operational costs. The catalytic performance of NiNPs in seawater was also found to be effective, further improving CO_2 absorption rates.

However, those studies utilized different concentrations of NiNPs and various surfactants or polymers to suspend the nanoparticles in the base solution (DI or seawater). Therefore, it was necessary to optimize the behavior of NiNPs in different concentrations of stabilizers along with their size to achieve the best results.

The stability of nanoparticles is the most important criterion for their performance. NiNPs have been used with three major stabilizing agents: PVP, CMC, and dextran (**Figure 5**). Research has found that CMC stabilizers show better performance for NiNP stability compared to PVP and dextran [33]. However, the optimization of the concentration of NiNPs along with the concentration of CMC in seawater has still not been investigated.

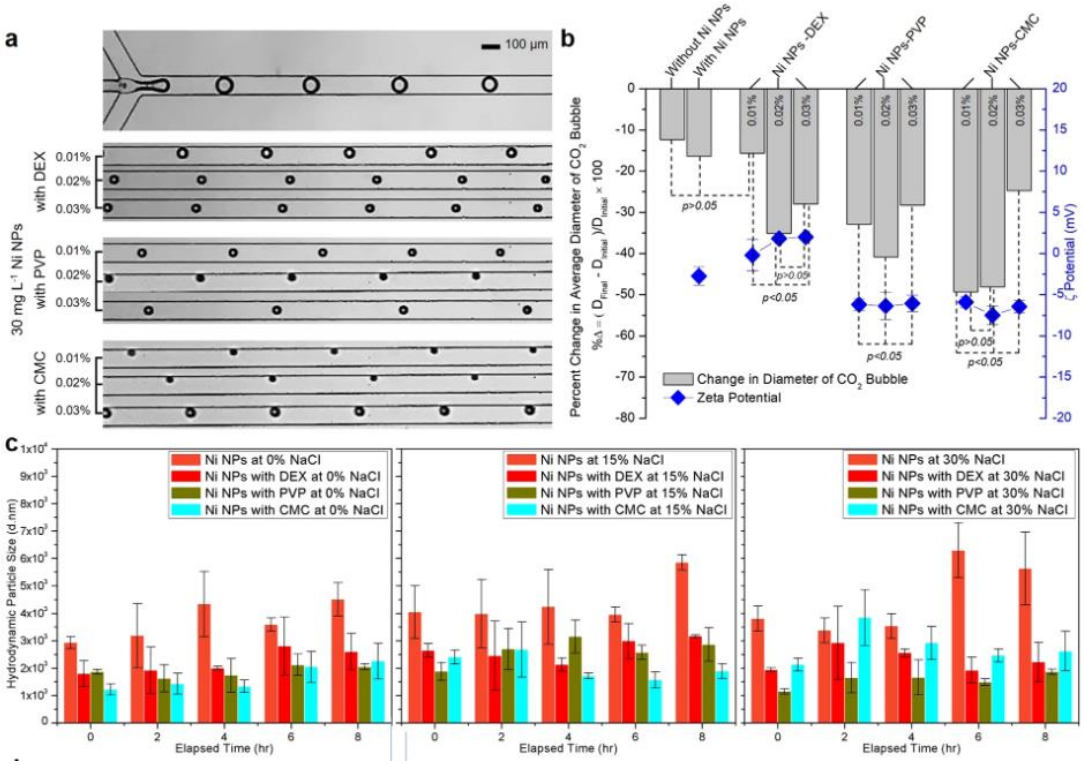

Figure 5:(a) Representative micrographs of CO2 bubbles near the junction (top) and the outlet (bottom) at stabilized Ni NPs by 0.01%, 0.02%, and 0.03% of DEX, PVP, and CMC at 10% NaCl.. (b) A diagram of percent changes in average diameter of CO2 bubbles in Ni NP

3. OBJECTIVE

The main objective of this study is to determine the optimal concentrations of NiNPs and CMC that maximize the dissolution of CO_2 in natural seawater. This research explored the synergistic effects of these agents in enhancing CO_2 solubility, a crucial factor in mitigating the impacts of atmospheric CO_2 on marine environments. By systematically varying the concentrations of NiNPs and CMC, I identified the most effective combination for accelerating CO_2 dissolution. This goal was achieved by investigating the underlying CO_2 dissolution mechanisms and surface chemistry during the reactions in a microchannel.

CO_2 dissolution in any process is associated with the physical parameters like pressure and temperature of the environment and the chemical properties of solvent like pH. When it comes to incorporation of nanotechnology in this process, unique physical and chemical properties of nanoparticles, such as a high surface area to volume ratio and enhanced reactivity can improve CO_2 solubility and its dissolution rate.

4. MATERIAL AND METHODS

4.1 CHEMICALS

Seawater was obtained from the Atlantic Ocean coastal areas of Boca Raton, Florida, with a measured salinity of 34 ± 1 ppt. NiNPs (Sigma Aldrich, St. Louis, MO) with an average diameter of 100 nm was used for all the solutions. The 300 nm diameter NiNPs (Sky Spring Nanomaterials, Inc., Houston, Tx) were also tested. The Carboxymethyl Cellulose sodium salt (CMC) polymers were purchased from Thermo Fisher Scientific Inc. The microfluidic chip was made from Polydimethylsiloxane (PDMS) elastomer kits (Sylgard 184, Dow Corning).

4.2 MICROCHIP PRODUCTION AND DESIGN

A microfluidic approach was utilized to analyze CO_2 absorption in the test solutions. Microbubble-based CO_2 absorption measurement in microfluidic platforms has a strong validation background in the literature [28,29,33]. It offers a tremendous experimental framework with easy and precise control over variables like pressure and flow rate. High-speed microscopic imaging was used to see the time-dependent size change of CO_2 microbubbles, which is a direct result of CO_2 absorption by the surrounding media. Hence, the CO_2 dissolution in the test solutions can be precisely determined by the change in size of the CO_2 microbubble over time. **Figure 6** shows an image of the microchannel utilized in all experiments to observe the CO_2 microbubbles. Furthermore, compared to

conventional experimental approaches, this microfluidic approach is far less expensive and more ecologically friendly because it necessitates substantially fewer resources.

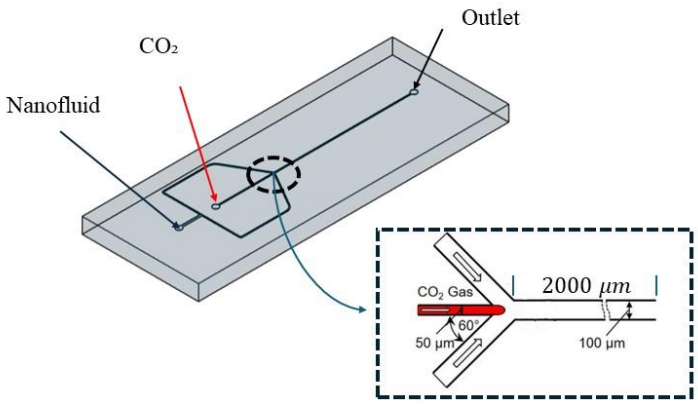

Figure 6: Flow focusing microfluidic device.

Photolithography and soft lithography were combined to create a microfluidic chip with microchannel geometry. In order to construct a photomask with the intended geometry, microchannel geometries were developed using computer-aided design (CAD) software (AutoCAD 2017, Autodesk, Inc., Sausalito, CA) and printed on a transparent sheet. CO_2 microbubbles were created due to flow-focusing microchannel shape **(Figure 6)**. With conventional photolithography, the mold design was printed on a silicon wafer (University Wafer, Inc., Boston, MA). Initially, a photoresist was spin-coated on a silicon wafer and heated by the hot plate. Subsequently, the photomask patterns with the designed geometry were transferred to the silicon wafer by exposing them to UV light. (**Figure 7**).

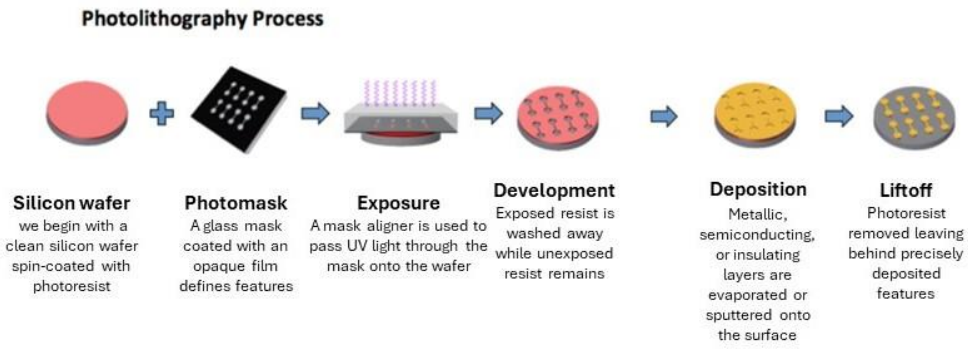

Figure 7: Process of making silicon wafer.

After mold development, microfluidic chips were fabricated by mixing PDMS with a silicone elastomer curing agent (10:1 w/w) and casting it into a master mold. PDMS was used because it is chemically and biologically inert and emits visible light well. Then, the PDMS-filled mold was degassed to remove the trapped air bubbles. Trapped air bubbles could lead to a pore visibility issue while an experiment is being performed. After degassing the PDMS solution in the mold, it became completely transparent, and without any trapped air bubbles, it was placed into the oven at 70 °C for one hour for curing. The cured PDMS was then peeled off the silicon wafer (master mold), and a 1.5 mm diameter biopsy punch punched the inlet and outlet ports. Lastly, after performing an oxygen plasma treatment, the PDMS chip was bonded with a glass microscope slide.

4.3 EXPERIMENTAL PROCEDURE

CO_2 gas was injected into a microfluidic chip with a flow-focusing geometry and an aqueous test solution. In the chip, CO_2 microbubbles were generated at the Y junction, where the solution flows at 60° angles with respect to the CO_2 flow stream. This arrangement of flows creates CO_2 bubbles at the microscale in the aqueous solution. By changing the flow rate and CO_2 inlet pressure, the CO_2 microbubble generation frequency

can be changed. In these experiments, the pressure and flow rate are fixed for the relative study of different solutions. The CO_2 pressure and flow rate of the test solutions were maintained at 4 Psig and 35 $\mu m/min$, respectively, throughout all the experiments. A total of 27 test solutions were used, combining varying weights of the CMC and NiNPs to have varying concentrations 0.1 %, 0.2 % and 0.3% (w/v) and, 0.006%, 0.008%, 0.01%,

0.03%, 0.05%, 0.07%, 0.09%, 0.150%, and 0.170% (w/v). The Nanoparticles were homogeneously dispersed in the seawater-based CMC solution with the help of an ultrasonicator. The ultrasonic rod was submerged into the solution with a sonication frequency of 20kHz for 30 minutes with 30 seconds per minute resting intervals to avoid overheating of the solution. The increase in temperature could lead to denaturing the CMC function.

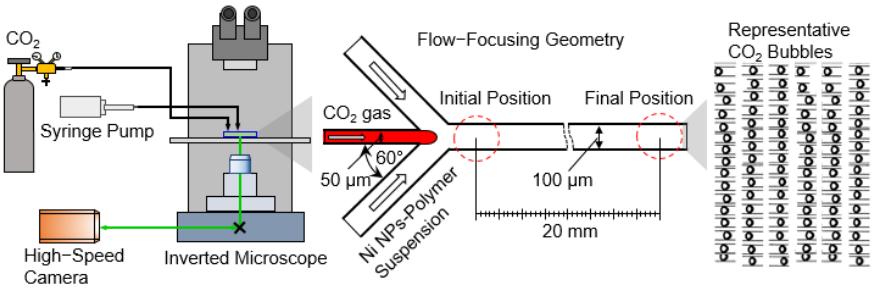

Figure 8: Illustrative diagram of experimental setup.

4.4 IMAGE PROCESSING

Each experiment was recorded at 2500 frames per second for 1 second. These videos were then analyzed to evaluate the bubble size at the beginning of formation at the flow-focusing Y-junction and at the outlet of the channel after the CO_2 microbubble traveled 2000 μm.

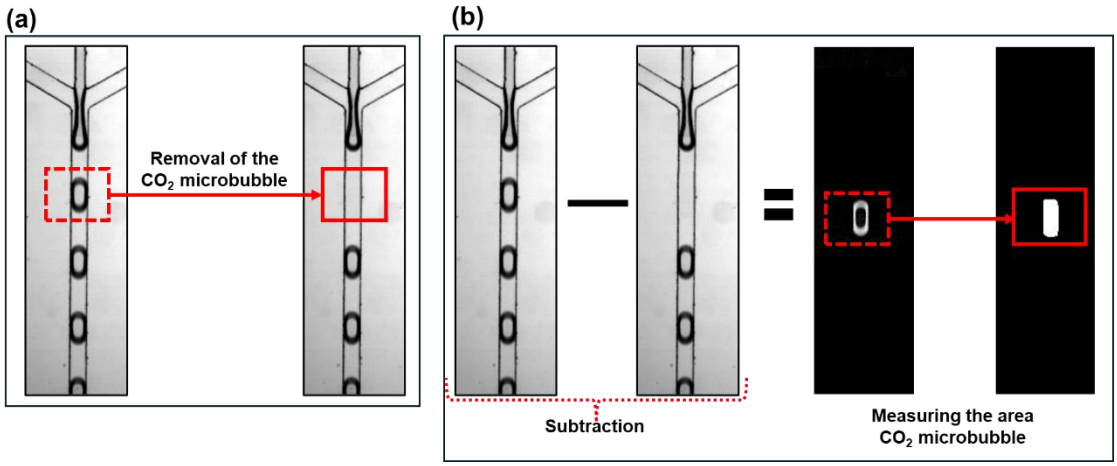

Figure 9: Demonstrating the processing for image analysis.

During this travel, the CO_2 dissolves into the surrounding solution, and the shrinkage in microbubble size provides an accurate estimate of CO_2 dissolution in the given solution.

To process the recorded videos, the initial frame in each video was processed using ImageJ software. The initial bubble was manually removed from the first frame to create a reference frame. Subsequently, as shown in **Figure 9**, this reference frame was subtracted from all the frames in that particular video using MATLAB. This process removed the microchannel wall and other noise, leaving only the pixels containing the CO_2 bubble, whose area was then easily measured. After obtaining the average area of the CO_2 microbubble, the difference between the initial and final areas was used to determine the total CO_2 dissolution for that particular trial.

As mentioned earlier, all experiments were conducted in triplicate. In each trial, 150 microbubbles at the initial site and at the end of the channel were analyzed, and their average area was recorded. **Figure 10** shows the image-processed data of CO_2 microbubble areas at the initial and endpoint for all three trials of the experiment conducted with a 300 mg/L CMC concentration and a 90 mg/L NiNP concentration. In the first trail the average

size of initial and final CO_2 microbubble were 508 pixel^2 and 146 pixel^2. For the second and third trial those values were 574 pixel^2 to 108 pixel^2 and 541 pixel^2 to 185 pixel^2 respectively.

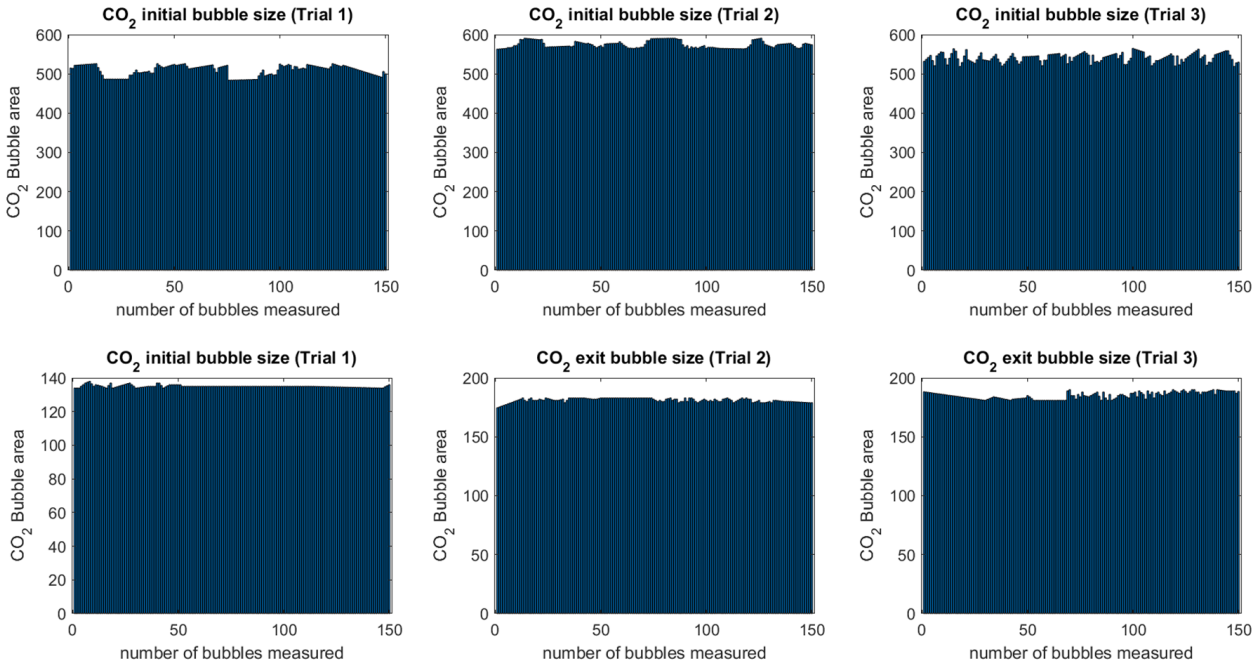

Figure 10: Subplots representing histograms of CO_2 bubble sizes at the beginning and end of the channel for all different trials.

5. RESULTS AND DISCUSSION

5.1 CO_2 DISSOLUTION PROCESS WITH NINP CATALYTIC ACTIVITY

CO_2 dissolution in a liquid solution follows a particular pH related dissociation pathway. Initially, CO_2 gas dissolves in the liquid, forming aqueous CO_2. This dissolved CO_2 then dissociates into bicarbonate ions, which further dissociate into carbonate ions in elevated pH environments. The chemical equations representing these processes are as follows [35]:

$$CO_2\ (g) \rightarrow CO_2\ (aq)$$

$$CO_2\ (aq) + H_2O \rightarrow H_2CO_3$$

$$H_2CO_3 \rightarrow H^+ + HCO_3^-$$

$$HCO_3^- \rightarrow H^+ + CO_3^{2-}$$

As indicated by these chemical equations, the dissolution of CO_2 makes the solution acidic and eventually leads to saturation with carbonate and bicarbonate ions, at which point the reaction stops. Upon the addition of NiNPs, each NiNP surface reacts with water molecules, forming bonds with hydroxyl groups (OH^-). This interaction enhances or catalyzes the dissociation of aqueous CO_2 into bicarbonate ions, as shown in the following equation:

$$NiNP + H_2O \rightarrow (NiNP - OH^-) + H^+$$

$$(NiNP - OH^-) + CO_2(aq) \rightarrow (NiNP - HCO_3^-)$$

$$(NiNP - HCO_3^-) + H_2O \rightarrow (NiNP - H_2O) + HCO_3^-$$

Eventually, the bicarbonate ions are replaced by water molecules on the surface of the NiNPs, allowing for their regeneration and continued catalytic activity. In **figure 11** the equation demonstrating how the NiNPs react in water as a catalyst can be illustratively below.

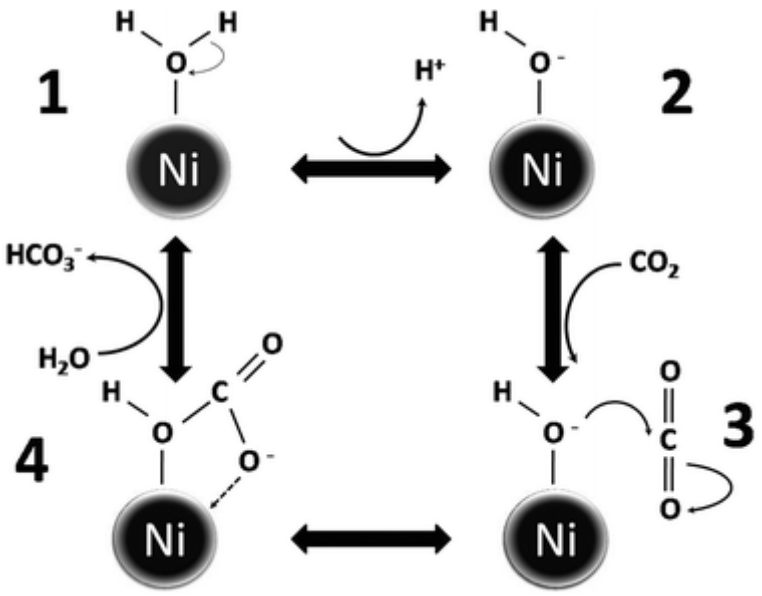

Figure 11: Schematic of the reaction mechanism of hydrogenation of CO2 by NiNPs.

In this literature by Bhaduri et al., it is noted that other forms NiNPs and their alloys can also support the hydration reaction of CO_2. This suggests that the catalytic properties of NiNPs are not limited to a single form, and various compositions and structures of NiNPs and their alloys can potentially enhance the hydration reaction of CO_2. This expands the possibilities for optimizing and utilizing different forms of NiNPs in carbon capture and storage technologies.

5.2 ANALYSIS OF CO_2 DISSOLUTION AT VARIOUS CMC AND NINP CONCENTRATIONS

To optimize the NiNPs and CMC concentrations, experiments were conducted with fixed CMC concentrations while varying the NiNPs concentrations. Starting with an arbitrary CMC concentration of 0.1% (w/v) in seawater, NiNPs concentrations of 0.01%, 0.03%, and 0.05% (w/v) were tested. As described in the experimental setup section, CO_2 dissolution was analyzed based on the reduction in CO_2 microbubble area.

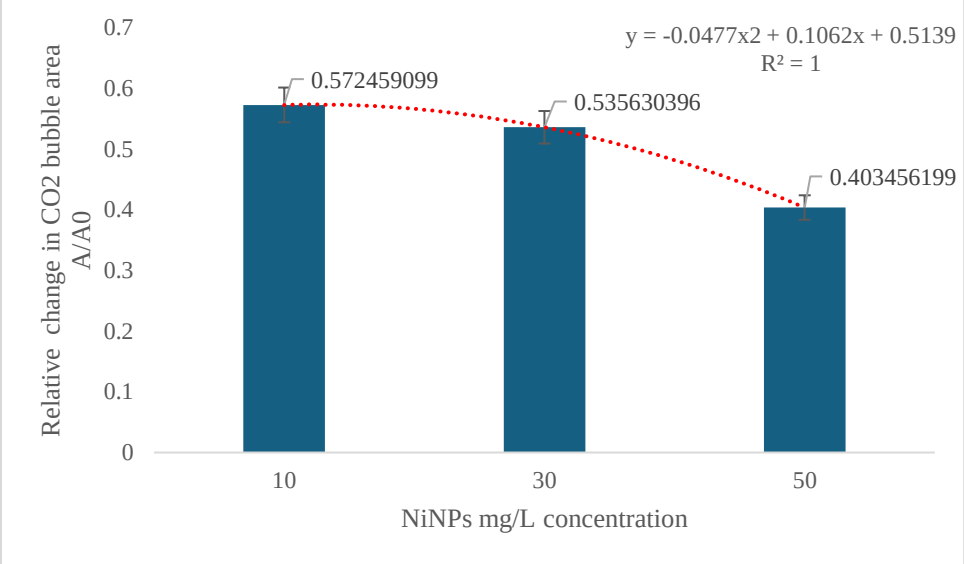

Figure 12: Demonstrates the dissolution rate of CO_2 at 0.1% (mg/L) CMC concentration.

The results of these experiments are depicted in **figure 12**. The x-axis represents the concentration of NiNPs, while the y-axis shows the average CO_2 size reduction across three trials. Error bars indicate the standard deviation of 3 trials, highlighting the variability and precision of the measurements. The figure graphically represents the relationship between NiNPs concentration and the rate of CO_2 dissolution in a 0.1% (mg/L) CMC concentration.

Figure 12 demonstrates a negative quadratic relationship between the concentration of NiNPs and the CO_2 bubble size reduction, revealing a downward trend as NiNPs concentration increases. The CO_2 bubble size reductions observed for NiNPs concentrations of 0.01%, 0.03%, and 0.05% (mg/L) were approximately 57.2%, 53.6%, and 40.3%, respectively. This trend suggests a complex interaction between the nanoparticles and the dissolution process. Lower concentrations of NiNPs may enhance the CO_2 size reduction by acting as nucleation sites, but higher concentrations reverse this effect, possibly due to particle agglomeration or the saturation of the CMC solution.

The observed decrease in CO_2 size reduction with increasing NiNPs concentration suggests an optimal nanoparticle concentration that maximizes dissolution, beyond which the efficacy is reduced. The initial enhancement of the CO_2 size reduction at lower concentrations of NiNPs could be attributed to an increased availability of nucleation sites. In contrast, the decline at higher concentrations might result from a reduced surface area available for dissolution due to particle agglomeration or the attainment of a saturation point in the seawater solution. This concept is further demonstrated in **figure 13.**

To further explore this theory, additional experiments were conducted with NiNPs concentrations of 0.006%, 0.008%, 0.70%, 0.90%, and 1.5% (mg/L). The CO_2 bubble size reductions observed for these concentrations were approximately 43.7%, 50.5%, 16.6%, 23.0%, and 18.4%, respectively (**figure 13**). This bell-shaped curve from the extended range of NiNPs concentrations supports the optimization hypothesis and enhances the understanding of the physicochemical interactions between nanoparticles and gas dissolution processes.

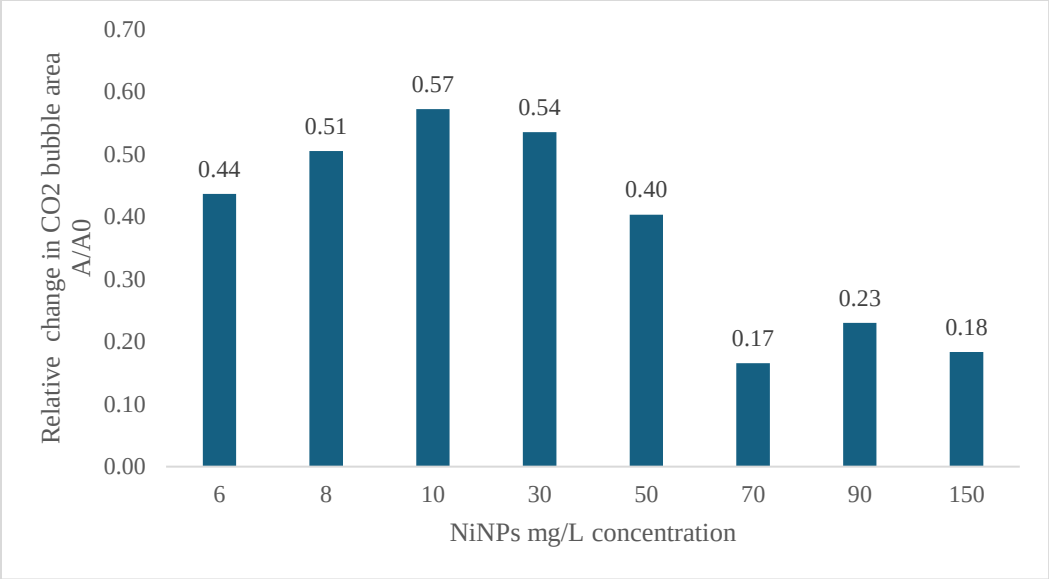

Figure 13: demonstrates the dissolute of CO2 a 0.1% (mg/L) CMC concentration

Additionally, at concentrations lower than the optimized 0.01% (mg/L), the reduction in CO_2 dissolution performance can be attributed to the higher CMC concentration relative to the NiNPs concentration. At lower concentrations, the nucleation sites may have been overwhelmed by the relatively higher CMC concentration, contrary to the effects observed at higher NiNPs concentrations.

For 100 nm-sized NiNPs in seawater, the optimized CO_2 dissolution was achieved at a CMC concentration of 0.1% (mg/L) with a NiNPs concentration of 0.01% (mg/L).

Similarly, at a CMC concentration of 0.2% (mg/L), NiNPs concentrations of 0.01% (mg/L), 0.03% (mg/L), and 0.05% (mg/L) were tested. **Figure 14** presents the dissolution rate of CO_2 in a solution with an increased CMC concentration of 200 mg/L, with the presence of NiNPs at concentrations of 10 mg/L, 30 mg/L, and 50 mg/L. The dissolution rates were measured at approximately 43.0%, 45.5%, and 52.0%, respectively. The trend observed here shows an initial decrease in the dissolution rate when the nanoparticle concentration

increases from 10 mg/L to 30 mg/L, followed by an increase at 50 mg/L. This non-linear interplay suggests a similar behavior to that observed at 100 mg/L CMC concentration.

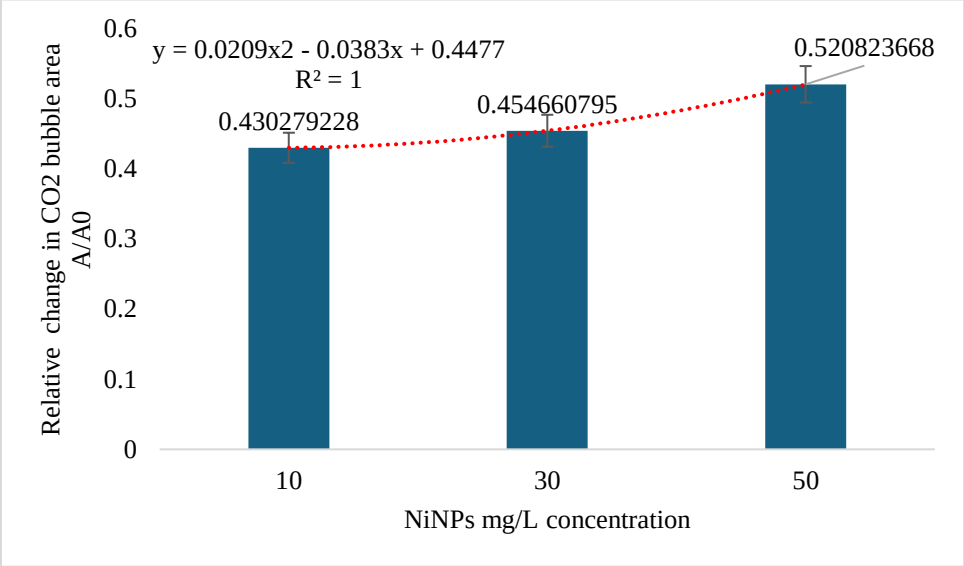

Figure 14: Demonstrates the dissolution rate of CO_2 at 0.2% (mg/L) CMC concentration.

To find the optimized value with the bell-shaped curve, the range of NiNPs concentration was then increased by adding 6 mg/L, 8 mg/L, 70 mg/L, 90 mg/L, and 150 mg/L as previously done. **Figure 15** shows the results of CO_2 dissolution as 17.0%, 32.0%, 58.0%, 52.0%, and 48.0% for NiNPs concentrations of 6 mg/L, 8 mg/L, 70 mg/L, 90 mg/L, and 150 mg/L, respectively. The optimized value found at 200 mg/L CMC concentration is 70 mg/L NiNPs concentration with 58% CO_2 dissolution. This value is nearly the same as the CO_2 dissolution achieved at 100 mg/L CMC concentration. The similar CO_2 dissolution at different NiNPs concentrations indicates the impact of a higher CMC concentration than required. This behavior can be reasoned similarly to the reduction of CO_2 dissolution at lower NiNPs concentrations.

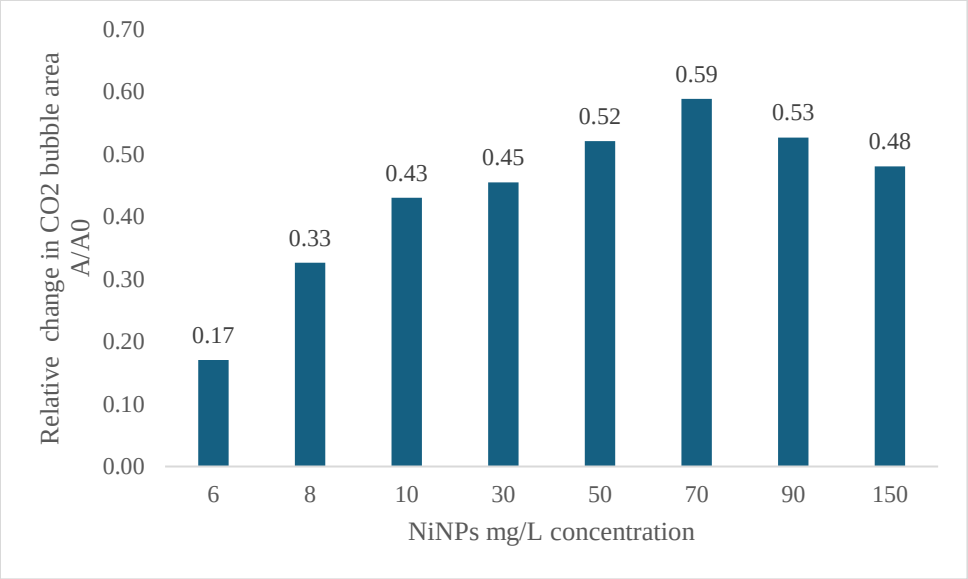

Figure 15: Demonstrates the dissolution rate of CO_2 at 0.2% (mg/L) CMC concentration.

Lastly, the CMC concentration was increased to 300 mg/L with a broad range of NiNPs concentrations to confirm the trend observed at 100 mg/L and 200 mg/L CMC concentrations. **Figure 16** shows the CO_2 dissolution at NiNPs concentrations of 6 mg/L, 8 mg/L, 10 mg/L, 30 mg/L, 50 mg/L, 70 mg/L, 90 mg/L, 150 mg/L, and 170 mg/L, which were found to be 12.0%, 15.0%, 46.0%, 51.0%, 53.0%, 60.0%, 67.0%, 53.0%, and 16.0%, respectively.

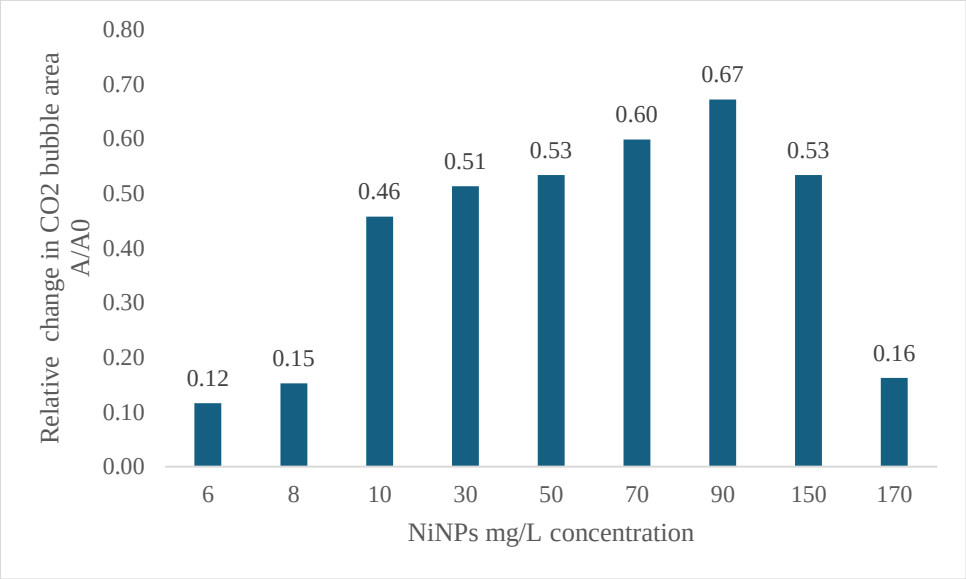

Figure 16: Demonstrates the dissolution rate of CO_2 at 0.3%(w/v) CMC concentration.

Figure 17 shows the overall experimental results at 100, 200, and 300 mg/L CMC concentrations with a broad range of NiNPs concentrations. When focusing on a 6 mg/L NiNPs concentration for all three CMC concentrations, the CO_2 dissolution rates are 44%, 17%, and 12%, respectively. The reduction in CO_2 dissolution with increasing CMC concentration at a particular NiNPs concentration can be attributed to an excess amount of CMC, which hinders the CO_2 dissolution and negatively affects the catalytic performance of the NiNPs. A similar trend is observed at an 8 mg/L NiNPs concentration.

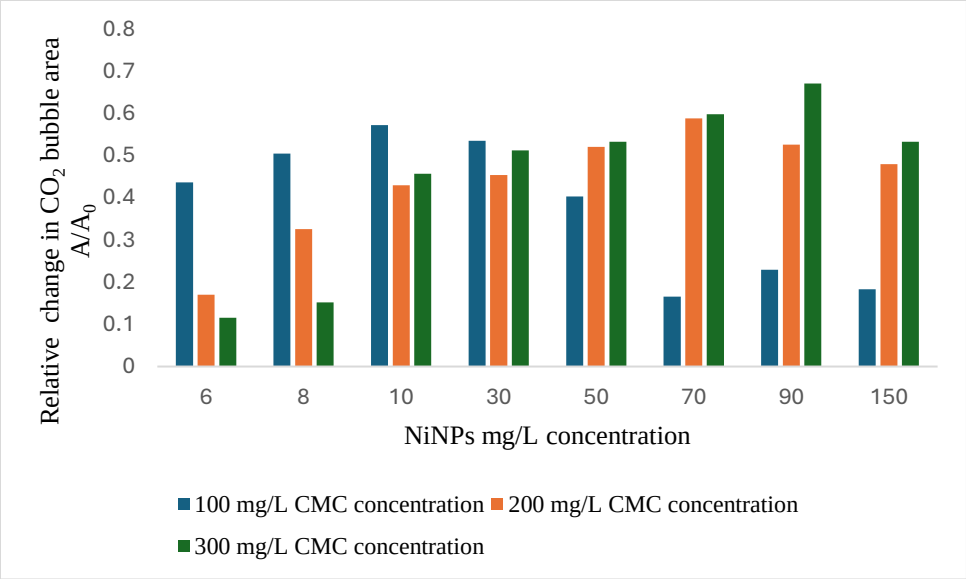

Figure 17: Demonstrates the dissolution rate of CO_2 for concentrations of CMC.

Conversely, at NiNPs concentrations above 50 mg/L, the trend shows the opposite direction. For example, at a 50 mg/L NiNPs concentration for CMC concentrations of 100 mg/L, 200 mg/L, and 300 mg/L, the CO_2 dissolution were approximately 40.3%, 52.0%, and 53.0%, respectively. The increase in CO_2 dissolution with increasing CMC concentration at a particular NiNP concentration above 50 mg/L for 100 mg/L CMC is likely due to the insufficient amount of CMC at higher concentrations of NiNPs, leading to the agglomeration of NiNPs and ultimately lower dissolution values. The opposite also holds true when dealing with NiNPs concentrations. To further explain this, for particular concentration of NiNPs, for example, from 6 mg/L to 10 mg/L there is a downward trend of CO_2 dissolution with the increase of CMC concentration. However, after the increase the concentration of CMC, the dissolution of CO_2 for the particular NiNPs concentration shows a positive trend which can be seen for concentrations 50 mg/L to 90 mg/L for the increases in CMC concentration. This observation reinforces the idea that there is an

optimal combination of CMC and NiNPs concentrations to achieve maximum CO_2 dissolution.

6. CONCLUSIONS

The catalytic activity of NiNPs (Nickel Nanoparticles) in CO_2 dissolution in seawater has garnered significant attention due to its environmentally friendly process, non-toxic solutions, conservation of freshwater, and the regenerative capability of NiNPs post-process. The stability of nanoparticles is crucial for their superior performance. Therefore, this research provides valuable insights into the solubility behavior of CO_2 in CMC (Carboxymethyl Cellulose) solutions augmented with NiNPs. Using a microfluidic approach, accurate CO_2 dissolution measurements were made at various concentrations of CMC and NiNPs, with two different sizes of NiNPs.

At CMC concentrations of 100 mg/L, 200 mg/L, and 300 mg/L, NiNPs concentrations of 6 mg/L, 8 mg/L, 10 mg/L, 30 mg/L, 50 mg/L, 70 mg/L, and 150 mg/L were investigated, respectively, for 100 nm-sized NiNPs. The experimental results demonstrated a bell-shaped curve for each set of NiNPs concentrations at each CMC concentration, indicating optimized NiNPs and CMC concentration behavior. It was found that a concentration of 10 mg/L NiNPs and 100 mg/L CMC showed an optimal CO_2 reduction of 57%. At a 200 mg/L CMC concentration, the highest CO_2 dissolution of 59% was achieved at 70 mg/L NiNPs concentration. Similarly, at a 300 mg/L CMC concentration, the highest CO_2 dissolution of 67% was achieved at 90 mg/L NiNPs concentration.

The results indicate that both the concentration of CMC and the amount of NiNPs significantly influence the dissolution rate of CO_2. While an increase in nanoparticle

concentration initially seemed to hinder the dissolution process in lower CMC solutions, higher CMC concentrations exhibited an improved dissolution rate. The observed trends highlight the delicate balance between the nanoparticle concentration and the medium's physicochemical properties, revealing a complex interplay that dictates the efficiency of CO_2 dissolution. These findings have implications for optimizing conditions in applications ranging from carbon capture to enhanced oil recovery.

Additionally, upon changing the NiNP diameter from 100 nm to 300 nm, the optimized trend shifted. At a 100 mg/L CMC concentration, the highest CO_2 dissolution was found at an 8 mg/L NiNPs concentration, whereas for the 100 nm diameter, it was at 10 mg/L. This shift to a lower concentration can be explained by the reduced surface area at a larger diameter of NiNPs. In other words, as the diameter increases, the total surface-to-volume ratio decreases, requiring less CMC to stabilize these particles. Future studies should aim to investigate the optimal size of nickel nanoparticles for maximizing CO_2 dissolution to enhance the efficiency of industrial processes.

6.1 FUTURE RECOMMENDATIONS

- Scaling up: Extend the microscale studies to large-scale experiments to verify if similar results can be obtained.
- Nanoparticle regeneration: Investigate methods for regenerating the nanoparticles used in the process, both at micro and large scales.
- Algae growth potential: Explore the possibility of using the CO_2-enriched seawater as an optimal environment for algae cultivation. This could potentially serve as a secondary benefit of the process.

REFERENCES

[1] IEA (2021), Global share of total energy supply by source, 2019, IEA, Paris https://www.iea.org/data-and-statistics/charts/global-share-of-total-energy-supply-by-source-2019, Licence: CC BY 4.0Buhre, B. J. P., Elliott, L. K., Sheng, C. D., Gupta, R. P., & Wall, T. F. (2005). Oxy-fuel combustion technology for coal-fired power generation. Progress in Energy and Combustion Science, 31(4), 283-307.

[2] Dugas, R. E. (2006). Pilot plant study of carbon dioxide capture by aqueous monoethanolamine. University of Texas at Austin.

[3] Hao, Y., Zhu, Q., Jiang, G., & Liu, L. (2015). Nanomaterials for the catalytic removal of NOx. Industrial & Engineering Chemistry Research, 54(25), 6417-6431.

[4] Higman, C., & van der Burgt, M. (2008). Gasification (2nd ed.). Gulf Professional Publishing.

[5] IPCC. (2018). Global Warming of 1.5°C. An IPCC Special Report on the impacts of global warming of 1.5°C above pre-industrial levels and related global greenhouse gas emission pathways.

[6] Kohl, A. L., & Nielsen, R. (1997). Gas Purification (5th ed.). Gulf Professional Publishing.

[7] Rao, A. B., & Rubin, E. S. (2002). A technical, economic, and environmental assessment of amine-based CO_2 capture technology for power plant greenhouse gas control. Environmental Science & Technology, 36(20), 4467-4475.

[8] Rochelle, G. T. (2009). Amine scrubbing for CO_2 capture. Science, 325(5948), 1652-1654.

[9] Wang, M., Lawal, A., Stephenson, P., Sidders, J., & Ramshaw, C. (2011). Post-combustion CO_2 capture with chemical absorption: A state-of-the-art review. Chemical Engineering Research and Design, 89(9), 1609-1624.

[10] Jansen, D., Gazzani, M., Manzolini, G., Dijk, E., & Carbo, M. (2015). Pre-combustion CO2 capture. *International Journal of Greenhouse Gas Control*, 40, 167-187.

[11] Theo, W. L., Lim, J., Hashim, H., Mustaffa, A., & Ho, W. S. (2016). Review of pre-combustion capture and ionic liquid in carbon capture and storage. *Applied Energy*, 183, 1633-1663.

[12] Dinca, C., Slavu, N., & Badea, A. (2017). Benchmarking of the pre/post-combustion chemical absorption for the CO2 capture. *Journal of the Energy Institute.*

[13] Pardemann, R., & Meyer, B. (2015). Pre-combustion carbon capture. In *Carbon Capture and Storage* (pp. 1-28). Wiley.

[14] Stanger, R., Wall, T., Spörl, R., Paneru, M., Grathwohl, S., Weidmann, M., Scheffknecht, G., Mcdonald, D., Myöhänen, K., Ritvanen, J., Rahiala, S., Hyppänen, T.,

Mletzko, J., Kather, A., & Santos, S. (2015). Oxyfuel combustion for CO2 capture in power plants. *International Journal of Greenhouse Gas Control, 40,* 55-125.

[15] Simmonds, M., Miracca, I., & Gerdes, K. (2005). Oxyfuel technologies for CO2 capture: A techno-economic overview. *International Journal of Greenhouse Gas Control*.

[16] Habib, M., Badr, H. M., Ahmed, S., Ben-Mansour, R., Mezghani, K., Imashuku, S., la O', G., Shao-horn, Y., Mancini, N., Mitsos, A., Kirchen, P., & Ghoneim, A. (2011). A review of recent developments in carbon capture utilizing oxy-fuel combustion in conventional and ion transport membrane systems. *International Journal of Energy Research, 35*.

[17] Kather, A., & Kownatzki, S. (2011). Assessment of the different parameters affecting the CO2 purity from coal fired oxyfuel process. *International Journal of Greenhouse Gas Control, 5*.

[18] Zheng, C., Liu, Z., Xiang, J., Zhang, L., Zhang, S., Luo, C., & Zhao, Y. (2015). Fundamental and technical challenges for a compatible design scheme of oxyfuel combustion technology. *Engineering, 1*(1), 139-149.

[19] Chao, C., Deng, Y., Dewil, R., Baeyens, J., & Fan, X. (2020). Post-combustion carbon capture. *Renewable & Sustainable Energy Reviews*.

[20] Fan, X. (2015). Post-combustion carbon capture. *Renewable & Sustainable Energy Reviews*.

[21] Wang, M., Lawal, A., Stephenson, P., Sidders, J., & Ramshaw, C. (2011). Post-combustion CO2 capture with chemical absorption: A state-of-the-art review. *Chemical Engineering Research & Design, 89*(9), 1609-1624.

[22] Mukherjee, A., Okolie, J., Abdelrasoul, A., Niu, C., & Dalai, A. (2019). Review of post-combustion carbon dioxide capture technologies using activated carbon. *Journal of Environmental Sciences, 83*, 46-63

[23] Liang, Z., Rongwong, W., Liu, H., Fu, K., Gao, H., Cao, F., Zhang, R., Sema, T., Henni, A., Sumon, K. Z., Nath, D., Gelowitz, D., Srisang, W., Saiwan, C., Benamor, A., Al-Marri, M., Shi, H., Supap, T., Chan, C. W., Zhou, Q., Abu-Zahra, M. R. M., Wilson, M., Olson, W., Idem, R., & Tontiwachwuthikul, P. (2015). Recent progress and new developments in post-combustion carbon-capture technology with amine based solvents. *International Journal of Greenhouse Gas Control, 40*, 26-54.

[24] Bounaceur, R., Lape, N. K., Roizard, D., Vallières, C., & Favre, É. (2006). Membrane processes for post-combustion carbon dioxide capture: A parametric study. *Energy, 31*(14), 2556-2570.

[25] Theo, W. L., Lim, J., Hashim, H., & Mustaffa, A. (2016). Review of pre-combustion capture and ionic liquid in carbon capture and storage. *Applied Energy, 183*, 1633-1663.

[26] Russo, M., Olivieri, G., Marzocchella, A., Salatino, P., Caramuscio, P., & Cavaleiro, C. (2013). Post-combustion carbon capture mediated by carbonic anhydrase. *Separation and Purification Technology, 107*, 331-339.

[27] Zhao, H., Luo, X., Zhang, H., Sun, N., Wei, W., & Sun, Y. (2018). Carbon-based adsorbents for post-combustion capture: a review. *Greenhouse Gases-Science and Technology, 8*(1), 11-36.

[28] Seo, S., Lages, B., & Kim, M. (2020). Catalytic CO2 absorption in an amine solvent using nickel nanoparticles for post-combustion carbon capture. *Journal of CO2 Utilization*, 36, 244-252.

[29] Ratanpara, A., Shaw, A., Thomas, M., Patel, R. N., & Kim, M. (2021). Microfluidic analysis of seawater-based CO2 capture in an amine solution with nickel nanoparticle catalysts. *Journal of CO2 Utilization, 53*, 101712. https://doi.org/10.1016/J.JCOU.2021.101712

[30] Hiremath, V., Shavi, R., & Seo, J. G. (2017). Mesoporous magnesium oxide nanoparticles derived via complexation-combustion for enhanced performance in carbon dioxide capture. *Journal of Colloid and Interface Science*, 498, 55-63

[31] Lee, J. W., Pineda, I., Lee, J. H., & Kang, Y. (2016). Combined CO2 absorption/regeneration performance enhancement by using nanoabsorbents. *Applied Energy*, 178, 164-176.

[32] Seo, S., Perez, G.A., Tewari, K. *et al.* Catalytic activity of nickel nanoparticles stabilized by adsorbing polymers for enhanced carbon sequestration. *Sci Rep* **8**, 11786 (2018).

[33] Hoya, R., & Fushimi, C. (2017). Thermal efficiency of advanced integrated coal gasification combined cycle power generation systems with low-temperature gasifier, gas cleaning and CO2 capturing units. *Fuel Processing Technology, 164*, 80-91.

[34] Emun, F., Gadalla, M., Majozi, T., & Boer, D. (2010). Integrated gasification combined cycle (IGCC) process simulation and optimization. *Computers & Chemical Engineering, 34,* 331-338.

[35] Bhaduri, G., & Šiller, L. (2013). Nickel nanoparticles catalyse reversible hydration of carbon dioxide for mineralization carbon capture and storage. *Catalysis Science & Technology, 3*(5), 1234-1239.